Discovery of Spin-Crossover Materials with Equivariant Graph Neural Networks and Relevance-Based Classification

Angel Albavera-Mata, Pawan Prakash, Jason B. Gibson, Eric Fonseca, Sijin Ren, Xiao-Guang Zhang, Hai-Ping Cheng, Michael Shatruk, S. B. Trickey,* and Richard G. Hennig*

Read Online

ACCESS | Metrics & More | Article Recommendations | Supporting Information

ABSTRACT: Swift discovery of spin-crossover materials for their potential application in electronic and quantum devices requires techniques that enable efficient identification of suitable candidates. To this end, we screened the Cambridge Structural Database to develop a specialized database of 1439 materials and computed spin-switching energies from density functional theory for each material. The database was used to train an equivariant graph convolution neural network to predict the magnitude of the spin-conversion energy. A test mean absolute error was 360 meV. For candidate identification, we equipped the system with a relevance-based classifier. This approach leads to a nearly 4-fold improvement in identifying potential spin-crossover systems of interest as compared to conventional high-throughput screening.
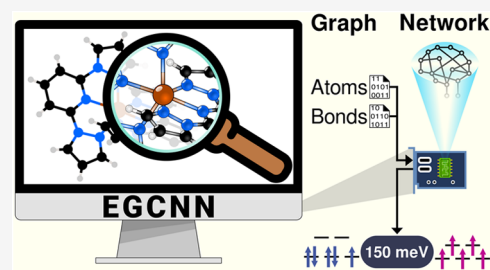
INTRODUCTION

First transition row $3d^4$ to $3d^7$ metal complexes may exhibit reversible switching from a low-spin to a high-spin state.[1,2] Unlike high-spin molecular magnets, for these types of complexes, two dominant effects compete during the spin conversion, namely, the electronic occupation of the d orbitals according to Hund's rule, and the filling of the t_{2g} lowest energy level. These mutually exclusive contributions result in two possible ground states that are directly dependent on the strength of the ligand field. More specifically, for strong ligand fields, the electrons preferably occupy the t_{2g} orbitals, leading to a low-spin state. For weak ligand fields, the electrons occupy the maximum number of orbitals, according to Hund's rule, which results in a high-spin state. Interestingly, whenever the strength of the ligand field and the electron pairing energy share nearly the same order of magnitude, a small external perturbation can overcome either effect and switch a metal complex to a low- or high-spin state.[3] The attractive feature of such reversible switching is its potential use in display devices, mechanical actuators, high-density memory storage, optoelectronics, sensing devices, or spintronics.[4−16]

From a computational perspective, these materials pose a challenge even to high-level wave function theories.[17−24] There are many considerations, one of which is that the accuracy scale of these high-level theories is comparable to the typical energy difference between the two spin states of approximately 10 kJ mol^{-1}, or about 100 meV. This difference, in turn, is close to the accuracy scale of the electronic structure method of choice.[25,26]

From the synthesis perspective, the vast combinatorial chemical space engendered by the metallic core, ligands,

coordination number, functional groups, size of the complex, strength of the intra- and intermolecular interactions, etc., poses a major challenge to efficient large-scale screening for the selection of promising materials suitable for specific applications.[27−30]

Development of machine learning strategies for elucidating the intricacies of the relationships between this vast material space and the spin-splitting energy is an active area of research.[31−33] Reference 34 highlights the complexity of such endeavors. Additionally, because of limited reports of experimental spin-crossover pursuits that ended up not finding spin-switching materials, it is arguable that the diversity of materials and availability of experimental data limits the extent to which general trends can be identified and applied.[35,36] As a result, a compromise takes precedence, namely, to restrict data to experimental observations[37] or use results from high-throughput computations.[33,38] Refined learning from experiments may be achieved by considering only specific families of materials of interest, at the cost of losing transferability to complexes of varying nature and of not being able to account for unsuccessful candidate materials. Conversely, high-throughput calculations of the spin-crossover energy with, for example, the Kohn−Sham density functional theory, are feasible. No general protocol exists, however, to select an

adequate exchange-correlation density functional approximation, a choice crucial to the accuracy of the results.[39−44]

Database screening is one of the more popular approaches for culling material candidates. With numerous samples, each of which involves large complicated molecules, machine learning techniques such as decision trees, kernel-based algorithms, or artificial neural networks, can aid in uncovering structure−property relationships, thereby accelerating the identification of candidates with promising physical-chemical properties.[45−48] Among these choices, graph neural networks provide a feasible architecture for encoding relevant physical and chemical descriptors for molecule-based and atom-based applications.[49−52] These advantages make graph models of particular interest for the description of spin-crossover materials.

This work thus is focused on assessing the performance of a specific type of graph model that is capable of learning the importance of symmetry representations,[53−55] namely, an equivariant graph convolutional neural network.[56,57] The task is the prediction of the sometimes elusive energy difference between the accessible spin states for a modest set of transition metal complexes. We show that such a network, with only 915 trainable parameters, can learn the relationship between the structure and the spin-state switching behavior for our data set. We provide evidence that the model achieves this ability by learning the importance of the coordination shells surrounding the metallic core. As proof of concept that the network provides an efficient instrument for candidate screening, and to demonstrate its usefulness, we screened a much larger data set of 11,356 transition metal complexes with between 13 and 280 atoms per molecule to identify 861 systems as promising candidates.

METHODOLOGY

We first describe the selection criteria for the material constituents of the data set obtained from the Cambridge Structural Database.[58] The screening strategy was implemented by identifying molecular structures containing Cr, Mn, Fe, or Co metal centers and excluding all materials with more than 50 non-hydrogen atoms in the asymmetric unit. Since a nontrivial number of the crystallographic files deposited to this database include disordered structures, missing hydrogen atoms, and unphysical moieties, among other imperfect systems, we examined and corrected individually the files to guarantee the integrity of the crystalline structures. Then fundamental properties of the resulting 1439 materials were computed via Kohn−Sham density functional calculations that used the r^{2}SCAN exchange-correlation functional approximation[59] since it has been shown to provide reasonable energy differences for metal complexes.[60] The electronic structure calculations used VASP 6.2,[61] with the set of projector augmented wave potentials for the outermost electrons as valence states, except for the transition metals, which were treated with the potentials that include the 4s semicore states as valence states. We set the plane wave kinetic energy cutoff to 520 eV and used an auxiliary support grid for the evaluation of the augmentation charges. The precision tolerance labeled as accurate was selected, nonspherical corrections were activated, and 10^{-6} and 10^{-3} eV were used as thresholds for the electronic steps and the Gaussian smearing width, respectively. All geometries were optimized with the conjugate gradient algorithm until force magnitudes were smaller than 10^{-2} eV

Å^{-1}. The rest of the computational parameters were left at default values.

With the purpose of targeting materials of interest for eventual technological applications such as were mentioned already,[4−16,32,34,62−66] it is essential that the spin transition in our study be characterized uniquely for the structure relaxations and the crossover energy of a candidate system of our interest. We required that the relevant spin-switching complexes satisfy three conditions, namely,

(1) the system ground state is low-spin,
(2) the spin and energy ordering of the states are consistent, i.e., the first excited state is high-spin, and
(3) the maximum low-spin to high-spin conversion energy per molecule is bounded to 500 meV, or nearly 4000 cm^{-1}.

The third criterion is generous, considering the error magnitudes commonly associated with electronic structure calculations for these materials.[67] The resulting distribution of the crystalline spin transition energies is depicted in Figure 1
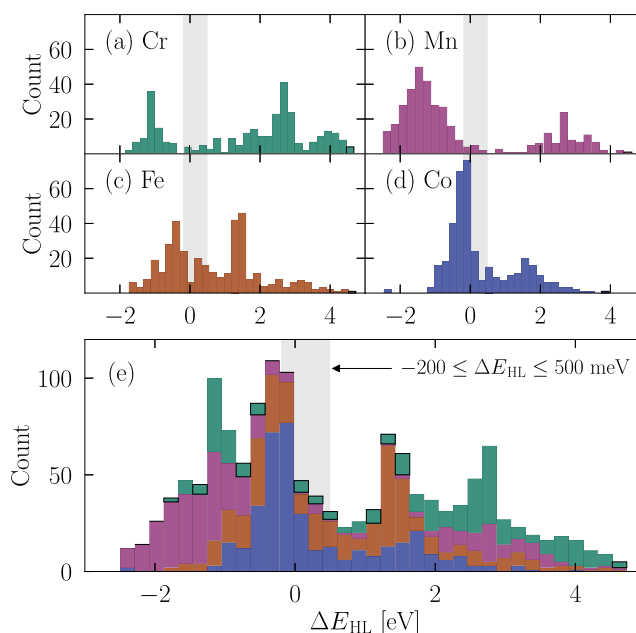

Figure 1. Distribution of the calculated crystalline spin-crossover energies per molecule for the 1439 species in the data set. Counts for each interval are depicted for (a) 316 Cr-, (b) 374 Mn-, (c) 372 Fe-, and (d) 377 Co-containing complexes, and (e) the data set as a whole. The shaded area illustrates the choice of the region of interest for spin-state switching candidates.

for 316, 374, 372, and 377 complexes with a Cr, Mn, Fe, and Co center, respectively. The data set has a mean spin-state switching energy of 538.5 meV and a standard deviation of 1.68 eV. The full list of entries is included in Table S1. The aforementioned energy differences are for crystalline computations that include crystal packing effects and counterions known for being crucial for proper thermodynamic description of these systems,[68] but to keep with standard spin-crossover analysis, for the eventual learning step, we isolated the molecular unit for each material based on the reported experimental coordinates, and assigned $-200 \leq \Delta E_{HL} \leq 500$ meV as the range of interest for spin-state switching candidates. Here, ΔE_{HL} is the spin-crossover energy for the metal complexes with total spin S increments given by

$$S = \begin{cases} 1 \rightarrow 2 & \text{for } 3d^4 \text{ ions } (Cr^{2+} \text{ and } Mn^{3+}) \\ \dfrac{1}{2} \rightarrow \dfrac{5}{2} & \text{for } 3d^5 \text{ ions } (Mn^{2+} \text{ and } Fe^{3+}) \\ 0 \rightarrow 2 & \text{for } 3d^6 \text{ ions } (Fe^{2+} \text{ and } Co^{3+}) \\ \dfrac{1}{2} \rightarrow \dfrac{3}{2} & \text{for } 3d^7 \text{ ion } (Co^{2+}) \end{cases} \quad (1)$$

The transition profile therefore can be represented as the total energy difference $\Delta E_{HL} = E_{HS} - E_{LS}$, where E_{LS} and E_{HS} are the total energy per molecule for the low-spin and high-spin states, respectively.

Regarding the choices for the machine learning model, we used the equivariant graph neural network as designed and implemented by Satorras, Hoogeboomand, and Welling,[56,57] but with a modified attention layer, ϕ_a, without coordinate embeddings, described below. This scheme considers the system of interest to be represented as a graph $\mathcal{G} = \mathcal{V} + \mathcal{E}$, with the set of nodes $v_i \in \mathcal{V}$ and the set of edges $\varepsilon_{i,j} \in \mathcal{E}$. We follow those authors' notation for clarity. Specifically for our purposes, for each system with N atoms, the feature node embeddings $\mathbf{h} \in \mathbb{R}^{N \times 1}$ list the atomic number z, whereas $\mathbf{x} \in \mathbb{R}^{N \times 3}$ correspond to the 3D Cartesian coordinates. Both $\mathbf{h}$ and $\mathbf{x}$ are associated with each of the graph nodes. We emphasize that, by design, this architecture preserves equivariance to translations and rotations on $\mathbf{x}$, and equivariance to permutations on the set $\mathcal{V}$. See Appendix A of ref 56 for proof.

To distinguish differences across distinct chemical functional groups, we also included the set of node attributes $\mathbf{v} \in \mathbb{R}^{V \times 1}$ and edge attributes $\mathbf{e} \in \mathbb{R}^{\mathcal{E} \times 1}$, that list the oxidation state for each node and bond order for each edge, respectively.[69] In particular, the oxidation state for each atom was determined by pairwise comparison of the electronegativity between its heteronuclear bonds, whereas the bond order is the sum of the products of the corresponding atomic orbital coefficients over all the occupied bands, rounded to its closest integer. The data set with these descriptors is available from the authors upon request. We restricted the model to a single convolutional layer to prevent overfitting due to the limited size of our data set. As a result, the model has only 915 learnable parameters. Furthermore, we used the nonlinear activation function known as *tanhshrink*, and trained the network for a maximum of 10^4 epochs with an early stop during validation.[70] The parameters were optimized with the adaptive moment estimation in stochastic gradient descent,[71] with a weight decay of 10^{-6}, considering an initial learning rate of 10^{-2}, and reduced on plateaus during training using a threshold of 1 meV.[72] Lastly, the edge attention $\alpha_{i,j}$ is defined as

$$\alpha_{i,j} = \phi_a(\mathbf{h}_i, \mathbf{h}_j \| \mathbf{e}_{i,j}) \quad (2)$$

where $\phi_a \in \mathbb{R}^3 \rightarrow \mathbb{R}^1$ is a weight matrix applied to every edge for the pair of nodes i, j, and $\|$ denotes the concatenation operation between $\mathbf{h}_i$, $\mathbf{h}_j$, and $\mathbf{e}_{i,j}$.

To establish a baseline model, we chose the gradient-boosting decision tree from the scikit-learn library.[73] The optimized hyperparameters using a grid search resulted in a learning rate of 7×10^{-2} using the Huber loss for a total number of 350 estimators.[74] The tree consists of a maximum depth of 64 estimators for a maximum splitting feature equal to

the square root of the number of features. We also used a minimum of four samples at a leaf node for a minimum of 52 samples required to split an internal node. The model is available from the authors upon request.

For both the graph network and baseline model, the whole data set was divided into 90% training fraction and 10% holdout fraction for testing. The 90% training set was used to optimize the hyperparameters using grid search in a 10-fold cross-validation without overlapping samples to ensure that each element is tested once. The training and testing splittings were identical for the two models. The behavior of the loss as a function of epochs for the neural network is depicted in Figure 2a. The training loss clearly decreases as the number of epochs
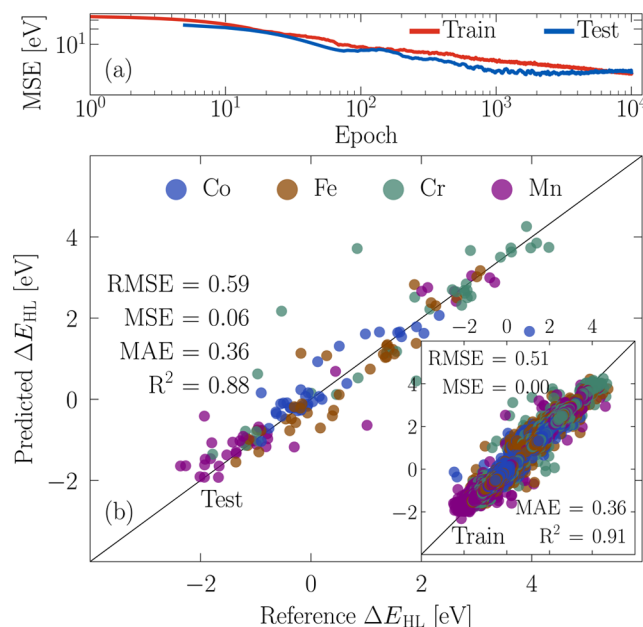

Figure 2. (a) Behavior of the mean signed error loss with a summation reduction as a function of epochs for the training and testing sets. (b) Correlation between the reference and predicted values by using the equivariant graph network for both the testing and training sets. The measures of central tendency are the root-mean-square error (RMSE), mean signed error (MSE), and mean absolute error (MAE). R^2 is the coefficient of determination.

increases. The testing loss, on the other hand, decreases during the first 70 epochs and then increases slightly through the following 130 epochs, followed by a second decrease as the number of epochs increases. After nearly 2000 epochs, the testing loss increases marginally and plateaus, showing early signs of overfitting. It is important to note that this is a retrospective analysis because, as stated previously, we did not implement an early stop for the final model. However, considering that the mean test loss increase with respect to epoch 2000 is on the order of 10^{-2} meV, the overfit can be safely disregarded.

RESULTS AND DISCUSSION

We begin with the evaluation of the predictive capability of the graph model. Comparisons for the agreement between the reference and predicted ΔE_{HL} values are reported in Figure 2b for the testing set. The training sample comparison is given in the inset. For statistical purposes, we used the interquartile range between the first and third quartile to characterize the

spread and variability of the predicted ΔE_{HL} for identification of outliers. The Cr-containing complexes show a total of four outliers, namely, LORBUQ, CYCPCR, ALUVIN, and CTNSCR; three for the Mn molecules, CAXTIH, UDOKON, and VEKFIA; three for Fe complexes, FIXSAH, HEYNEE, and CITCUD; and two for Co molecules, WIYJEV, and SETJEI. Most of the molecules containing Mn, Fe, and Co correspond to octahedral complexes and metallocenes. Putting that aside, although Figure 2a shows early signs of overfitting, we see reasonable agreement between the testing and training predictions reported in Figure 2b, indicating that the effects are minimal.

From an implementation perspective, our goals include learning chemically relevant features and understanding how the neural network makes the predictions. We expect the modified attention layer in eq 2 to be able to provide the means for distinguishing molecular sites that are more strongly associated with the spin transition from other sites.

With that in mind, we sampled a series of progressively more distant coordination shells surrounding the transition metal center, under the consideration that the largest number of admissible coordination shells must not exceed the number of neighboring atoms in a complex. In each case, subgraphs were built that included the nodes and edges of all the molecules in that set of shells. Figure 3 shows that both RMSE and R^2 converge rapidly as the number of coordination shells increases. Results remain nearly unchanged after five shells.
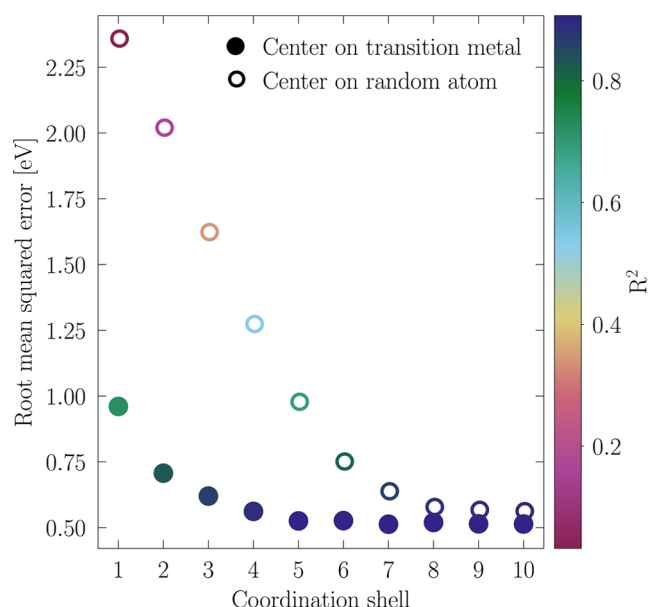

Figure 3. Behavior of the RMSE and R^2 as a function of graphs built with nodes and edges for sequentially increased numbers of coordination shell approximations. Two reference types were chosen, namely, coordination shells starting at the metallic center or at random atoms of the molecule. For both cases, the reference atom was kept fixed once it was picked.

A distinctly different trend is observed when a random atom is used as the coordination shell center. For that choice, Figure 3 shows that the mean errors roughly double, as does the number of coordination shells needed to achieve the same quality results as in the metal-centered case. The R^2 values also deteriorate. It must be noted, however, that since the data set includes medium-sized molecules, using 10 coordination shells

essentially covers the whole molecule for most of the samples. The contrasting tendencies for the two approaches nonetheless show that the network learned the local importance of the transition metal core dominance for the spin transition.

In addition, examining the characteristics of the element composition of the complex core may provide insights into the chemical features that the network learned to determine ΔE_{HL}. For that, we focused our attention on the first five coordination shells that show a more rapidly varying RMSE in Figure 3. For each progressively larger shell, we counted the total number of distinct elements and computed their cumulative summation, we then calculated the relative composition per element by dividing the element count by the total number of atoms in that shell. Figure 4 shows the results for such analysis, with
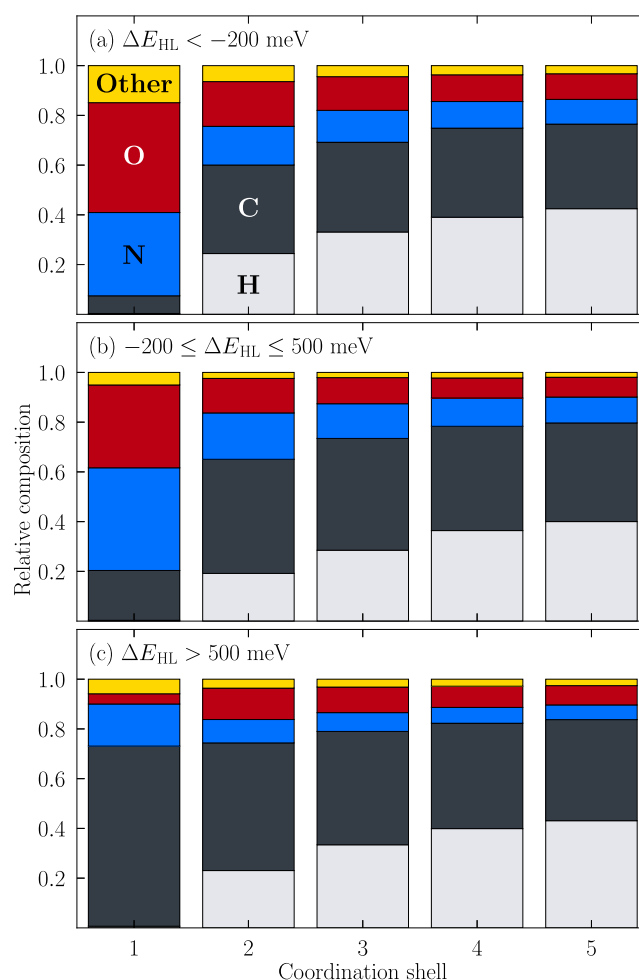

Figure 4. Relative compositions for carbon, nitrogen, oxygen, hydrogen, and other atoms, such as B, F, P, S, Cl, and I, as a function of the number of coordination shells centered on the transition metal for the species showing (a) high-spin states with $\Delta E_{HL} < -200$ meV, (b) spin-switching candidates, with $-200 \leq \Delta E_{HL} \leq 500$ meV, and (c) low-spin states $\Delta E_{HL} > 500$ meV.

particular emphasis on the hydrogen, carbon, nitrogen, and oxygen atoms that represent the largest compositions across all coordination shells.

For the purposes of the following discussion, we will omit the Hydrogen atoms because their relative composition increases rapidly with the number of coordination shells and because they do not provide meaningful information regarding ligand composition. The element decomposition for the

species identified as high-spin states is shown in Figure 4a. Here we observe that the O atom is most prominent, followed by N, and a noticeable presence of other atoms like B, F, P, S, Cl, or I. This composition agrees with the spectrochemical series,[75−79] where the weak field of ions such as O_2^{2-}, I^-, Br^-, Cl^-, NO_3^-, or F^- results in high-spin states.

For the species identified as spin-crossover candidates depicted in Figure 4b, on the other hand, we see nearly 3 times fewer weak-field atoms and a large presence of N and O atoms where N is the slightly more prominent element, as opposed to the lesser population of C atoms that increases for larger shell counts. These findings agree with the element composition of the typical ligands used to synthesize these metal complexes,[30,80−85] whereas the C atoms that appear in the first coordination shell can be attributed to the presence of metallocenes.

Regarding the low-spin species, Figure 4c shows that the C atoms account for roughly 75% of the total composition for the first coordination shell, followed by N, and a nearly equal composition of the O and other atoms that, however, becomes more populated by the O atoms for larger coordination shells. Once again, these findings agree with the spectrochemical series where the strong fields of ions such as CH_3CN, Cp^-, CN^-, and CO produce low-spin states.

The trends observed for N and O, for both spin-switching and nonspin-switching complexes depicted in Figure 4, remain nearly unchanged for a larger number of coordination shells, whereas the number of C atoms increases rapidly as we sample a larger subspace of the ligand structure.

The motivation for using coordination shells is to provide qualitative insight into the effects of ligand field stabilization. At the same time, the spin transitions of interest are modulated by a delicate balance between the metal ion properties and the strength of the ligand field,[25,40,86−93] in which vibrational contributions to the free energy must be taken into account for detailed representation of thermochemical behavior. Those considerations are well beyond the scope of the present work. Here we focus solely on using the energy difference for elucidating tendencies.

Because the motivation for constructing and training the network is its subsequent use to search for potential spin-crossover complexes, we needed to convert the regression into a classification model. Therefore, establishing the precision-recall trade-off becomes relevant. The precision measures the correctness of the model for actual spin-crossover predictions, whereas the recall is associated with how many relevant complexes the network recovers. We used the method proposed by Torgo and Ribeiro[94] to turn the continuous regression into a classification process. To do so, we must define the importance for the target class, termed relevance, through the use of a continuous relevance function scale that maps the original continuous domain to the discrete target class. Recall that the energy interval of interest, defined generously, is $-200 \leq \Delta E_{HL} \leq 500$ meV. A basic approach is to define the relevance $f(Y)$ for a given ΔE_{HL} by means of two sigmoid functions, one for the lower and another for the upper limit, expressed by

$$f(Y) = \frac{1}{1 + \exp[-s \cdot (Y - c)]} \qquad (3)$$

where c is the center of the sigmoid and defines the threshold where larger values of the target variable Y start to become more relevant. By construction, both thresholds have a

relevance equal to 1/2, as depicted in Figure 5a. The remaining variable s is related to the slope of the sigmoid
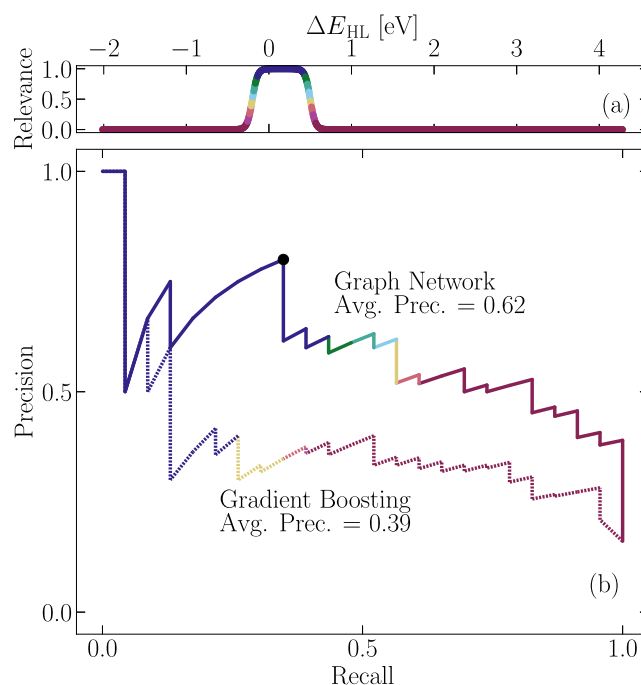

Figure 5. Classification of molecular metal complexes as potential candidates for spin crossover (a) based on the energy difference between the high-spin and low-spin states and (b) the precision-recall curve for the testing set as a function of the choice of relevance for the graph neural network and the gradient-boosting baseline method. Identical data splittings were used for both methodologies.

functions. It is fixed by the energy difference resolution, which we chose at 1 meV. Figure 5a shows clearly how the relevance is larger for energy differences in between the interval of interest and tends to zero otherwise.

Having stipulated the mapping between ΔE_{HL} and its relevance, the precision-recall curve, depicted in Figure 5b, is generated readily by determining the combinations between the true and false classes with positive and negative outcomes. Once more, we used the testing set for our analysis. Since we are interested in minimizing the number of redundant calculations, the optimum value for the relevance $f(Y)$ threshold is such that it maximizes the precision while retaining a reasonable recall. This choice is depicted with the dot in Figure 5b, which corresponds to a precision of nearly 80% and a recall of roughly 35% for a relevance of roughly 0.90. That, in turn, accounts for a difference of 68 meV with respect to the original lower and upper limits, resulting in the tighter $-132 \leq \Delta E_{HL} \leq 432$ meV interval and a false positive rate of just 1.7%.

In addition, use of Bayes' theorem shows a 56% probability for finding a predicted ΔE_{HL} that is within the range of interest. That corresponds to a 4-fold increase with respect to the 13% probability for random picking that pertains to the 167 species that meet the criterion in the training set. See the lower limit in Figure 5b for the full recall with a relevance of zero and the Supporting Information for details on the use of Bayes' theorem. For the sake of completeness, this same analysis can be extended to the opposite case, in which we measure the ability of the system to disregard molecules. We obtained a refusal probability of ≈94% that corresponds to an

approximate 17-fold reduction in the number of redundant Kohn−Sham density functional calculations, as obtained from the complement of this refusal probability, $1/(6 \times 10^{-2})$. These two probabilities show that the graph model increases the chances for finding materials of interest substantially while rejecting unsuitable complexes with confidence.

The simpler gradient-boosting baseline model results shown in Figure 5b demonstrate clearly different, inferior performance for the same testing set. The lower transferability of the baseline model becomes clear, with an average precision of approximately 40%. In a broader sense, Figure 5b unveils the effectiveness of using comparatively simple graph neural networks.

To test our graph neural network system on a much larger variety of mononuclear transition metal complexes, we collected a total of 11,356 such molecules from the Cambridge Structural Database spanning the range $13 \leq N_{\text{Atoms}} \leq 280$, where N_{Atoms} is the number of atoms per molecule, and used the graph neural network to predict ΔE_{HL}. The data are included in Table S2. The resulting distributions of the spin-state energy difference are shown in Figure 6a−d for molecules
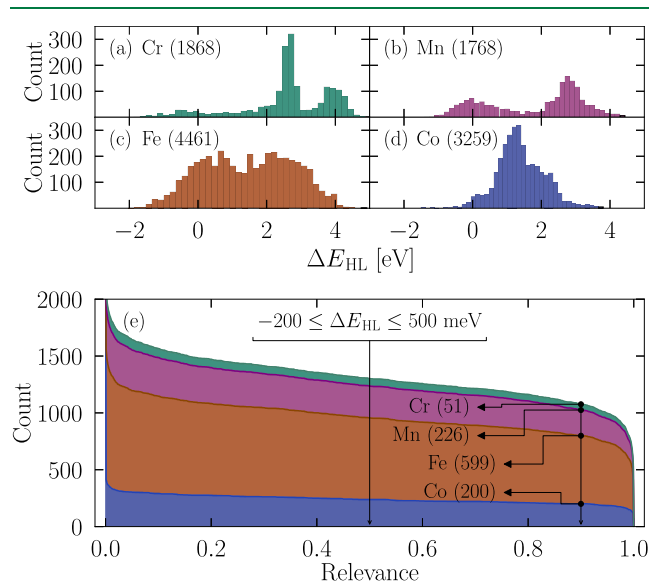

Figure 6. Predicted spin-crossover energies for mononuclear complexes containing (a) Cr, (b) Mn, (c) Fe, and (d) Co metal centers obtained from the Cambridge Structural Database, and (e) the total number of plausible candidates retrieved for increasingly tightened choices of relevance.

with Cr, Mn, Fe, and Co centers, respectively. Additionally, in Figure 6e we report the number of potential spin-switching species for the different metallic centers and extend our evaluation to the number of candidates retrieved as a function of the relevance criteria.

There are two asymptotic conditions depicted in Figure 6e, namely, a relevance equal to zero that essentially recovers all entries in the data set and a relevance equal to one with the opposite outcome. As a reminder, the boundary for the interval $-200 \leq \Delta E_{\text{HL}} \leq 500$ meV by construction is located halfway through. For that threshold, the classification results in 1301 species of interest. As stated previously, however, we may increase the precision of the neural network by tightening the relevance to, e.g., 0.9, and expect a decreasing recall because the model is not a perfect classifier. As a result, the final

population contains 1076 metal complexes with the potential to exhibit spin crossover, with the individual counts reported in Figure 6e. Considering that the test precision shown in Figure 5 is 80% for this value of relevance, approximately 861 of the 1076 materials predicted by our model are expected to have a ΔE_{HL} well within the range of interest, thus vastly accelerating the identification of material candidates. Interestingly, most of the recovered candidates are Fe-based molecules, independent of the relevance criteria. This disproportion is somewhat expectable because 4,461 such molecules constitute nearly 39% of the data set entries, as well as the majority with $-1 \leq \Delta E_{\text{HL}} \leq 1$ eV. They are followed in prominence by the Mn-based systems. These observations also fit well with the known propensity of the Fe(II) complexes to exhibit spin crossover behavior, as compared to complexes with other relevant metal ions.[82,95]

◼ CONCLUDING REMARKS

On the basis of a data set of 1439 medium-sized transition metal complexes extracted from the Cambridge Structural Database, we have achieved a graph network model for efficient screening of spin-state-conversion candidates. The model succeeds by combining descriptors that retain chemically relevant molecular information with an equivariant graph neural network and a subsequent classifier by relevance. Our evaluation shows that use of the neural network approximately quadruples the chances for finding metal complexes that might exhibit spin crossover, while confidently rejecting unsuitable molecules.

In this analysis, we assumed the spin-state conversion energy interval $-200 \leq \Delta E_{\text{HL}} \leq 500$ meV to be a reasonable compromise in view of the accuracy of the exchange-correlation approximation used to equip the data set. The assumption is of course debatable. The interval of interest depends strongly on the choice of electronic structure method for the computation of ΔE_{HL} and the zero-point energy corrections that were not included in our study. Our work, however, is not focused on addressing refined electronic structure calculations but rather on developing high-throughput alternatives to alleviate the computing burdens required for materials discovery. To this end, our graph model exhibits a competitive ability to exclude unsuitable materials that in turn results in approximately a 17-fold reduction of low-productivity computations.

◼ ASSOCIATED CONTENT

Ⓢ Supporting Information

The Supporting Information is available free of charge at https://pubs.acs.org/doi/10.1021/acs.jctc.4c01690.

> Detailed description for the different terms used in the discussion of Bayes' theorem and the two data sets used in this work. These data sets include the CSD identifier, ΔE_{HL}, and the transition metal center for every species listed therein. (PDF)

◼ AUTHOR INFORMATION

Corresponding Authors

S. B. Trickey − *Center for Molecular Magnetic Quantum Materials, Gainesville, Florida 32611, United States; Department of Physics and Department of Chemistry, University of Florida, Gainesville, Florida 32611, United*

States; ⓘ orcid.org/0000-0001-9224-6304;
Email: trickey@ufl.edu

Richard G. Hennig − *Center for Molecular Magnetic Quantum Materials, Gainesville, Florida 32611, United States; Department of Materials Science and Engineering, University of Florida, Gainesville, Florida 32611, United States;* ⓘ orcid.org/0000-0003-4933-7686;
Email: rhennig@ufl.edu

Authors

Angel Albavera-Mata − *Department of Physics, University of Florida, Gainesville, Florida 32611, United States; Center for Molecular Magnetic Quantum Materials, Gainesville, Florida 32611, United States;* ⓘ orcid.org/0000-0003-1521-678X

Pawan Prakash − *Department of Physics, University of Florida, Gainesville, Florida 32611, United States; Center for Molecular Magnetic Quantum Materials, Gainesville, Florida 32611, United States*

Jason B. Gibson − *Department of Materials Science and Engineering and Quantum Theory Project, University of Florida, Gainesville, Florida 32611, United States*

Eric Fonseca − *Center for Molecular Magnetic Quantum Materials, Gainesville, Florida 32611, United States; Department of Materials Science and Engineering, University of Florida, Gainesville, Florida 32611, United States*

Sijin Ren − *Center for Molecular Magnetic Quantum Materials, Gainesville, Florida 32611, United States; Department of Materials Science and Engineering, University of Florida, Gainesville, Florida 32611, United States*

Xiao-Guang Zhang − *Department of Physics, University of Florida, Gainesville, Florida 32611, United States; Center for Molecular Magnetic Quantum Materials, Gainesville, Florida 32611, United States;* ⓘ orcid.org/0000-0003-0092-5006

Hai-Ping Cheng − *Center for Molecular Magnetic Quantum Materials, Gainesville, Florida 32611, United States; Department of Physics, Northeastern University, Boston, Massachusetts 02115, United States;* ⓘ orcid.org/0000-0001-5990-1725

Michael Shatruk − *Center for Molecular Magnetic Quantum Materials, Gainesville, Florida 32611, United States; Department of Chemistry and Biochemistry, Florida State University, Tallahassee, Florida 32306, United States*

Complete contact information is available at:
https://pubs.acs.org/10.1021/acs.jctc.4c01690

Notes

The authors declare no competing financial interest.

■ REFERENCES

(1) Gütlich, P.; Hauser, A. *Spin Crossover in Transition Metal Compounds I*; Springer, 2004; pp 1−47.

(2) Hauser, A. *Spin Crossover in Transition Metal Compounds I*; Springer, 2004; Vol. 233, pp 49−58.

(3) Nicolazzi, W.; Bousseksou, A. Thermodynamical aspects of the spin crossover phenomenon. *C. R. Chim.* **2018**, *21*, 1060−1074.

(4) Kahn, O.; Kröber, J.; Jay, C. Spin Transition Molecular Materials for displays and data recording. *Adv. Mater.* **1992**, *4*, 718−728.

(5) Kahn, O.; Martinez, C. J. Spin-Transition Polymers: From Molecular Materials Toward Memory Devices. *Science* **1998**, *279*, 44−48.

(6) Garcia, Y.; Ksenofontov, V.; Gütlich, P. Spin Transition Molecular Materials: New Sensors. *Hyperfine Interact.* **2002**, *139−140*, 543−551.

(7) Muller, R. N.; Vander, E. L.; Laurent, S. Spin Transition Molecular Materials: Intelligent Contrast Agents for Magnetic Resonance Imaging. *J. Am. Chem. Soc.* **2003**, *125*, 8405−8407.

(8) Létard, J.-F.; Guionneau, P.; Goux-Capes, L. *Spin Crossover in Transition Metal Compounds III*; Springer, 2004; Vol. 235, pp 221−249.

(9) Larionova, J.; Salmon, L.; Guari, Y.; Tokarev, A.; Molvinger, K.; Molnár, G.; Bousseksou, A. Towards the Ultimate Size Limit of the Memory Effect in Spin-Crossover Solids. *Angew. Chem., Int. Ed.* **2008**, *47*, 8236−8240.

(10) Sanvito, S. Molecular spintronics. *Chem. Soc. Rev.* **2011**, *40*, 3336−3355.

(11) Quintero, C. M.; Félix, G.; Suleimanov, I.; Sánchez Costa, J.; Molnár, C. J. S. G.; Molnár, G.; Salmon, L.; Salmon, L.; Nicolazzi, W.; Nicolazzi, W.; Bousseksou, A. Hybrid spin-crossover nanostructures. *Beilstein J. Nanotechnol.* **2014**, *5*, 2230−2239.

(12) Ruiz, E. Charge transport properties of spin crossover systems. *Phys. Chem. Chem. Phys.* **2014**, *16*, 14−22.

(13) Jureschi, C. M.; Linares, J.; Rotaru, A.; Ritti, M. H.; Parlier, M.; Dîrtu, M. M.; Wolff, M.; Garcia, Y. Pressure Sensor via Optical Detection Based on a 1D Spin Transition Coordination Polymer. *Sensors* **2015**, *15*, 2388−2398.

(14) Manrique-Juárez, M. D.; Rat, S.; Salmon, L.; Molnár, G.; Quintero, C. M.; Nicu, L.; Shepherd, H. J.; Bousseksou, A. Switchable molecule-based materials for micro- and nanoscale actuating applications: Achievements and prospects. *Coord. Chem. Rev.* **2016**, *308*, 395−408.

(15) Mikolasek, M.; Manrique-Juarez, M. D.; Shepherd, H. J.; et al. Complete Set of Elastic Moduli of a Spin-Crossover Solid: Spin-State Dependence and Mechanical Actuation. *J. Am. Chem. Soc.* **2018**, *140*, 8970−8979.

(16) Cruddas, J.; Powell, B. J. Multiple Coulomb phases with temperature-tunable ice rules in pyrochlore spin-crossover materials. *Phys. Rev. B* **2021**, *104*, No. 024433.

(17) Daku, L. M. L.; Aquilante, F.; Robinson, T. W.; Hauser, A. Accurate Spin-State Energetics of Transition Metal Complexes. 1. CCSD(T), CASPT2, and DFT Study of $[M(NCH)_6]^{2+}$ (M = Fe, Co). *J. Chem. Theory. Comput.* **2012**, *8*, 4216−4231.

(18) Droghetti, A.; Alfé, D.; Sanvito, S. Ground state of a spin-crossover molecule calculated by diffusion Monte Carlo. *Phys. Rev. B* **2013**, *87*, No. 205114.

(19) Song, S.; Kim, M.-C.; Sim, E.; Benali, A.; Heinonen, O.; Burke, K. Benchmarks and Reliable DFT Results for Spin Gaps of Small Ligand Fe(II) Complexes. *J. Chem. Theory. Comput.* **2018**, *14*, 2304−2311.

(20) Phung, Q. M.; Feldt, M.; Harvey, J. N.; Pierloot, K. Toward Highly Accurate Spin State Energetics in First-Row Transition Metal Complexes: A Combined CASPT2/CC Approach. *J. Chem. Theory. Comput.* **2018**, *14*, 2446−2455.

(21) Flöser, B. M.; Guo, Y.; Riplinger, C.; Tuczek, F.; Neese, F. Detailed Pair Natural Orbital-Based Coupled Cluster Studies of Spin Crossover Energetics. *J. Chem. Theory Comput.* **2020**, *16*, 2224−2235.

(22) Zhang, D.; Truhlar, D. G. Spin Splitting Energy of Transition Metals: A New, More Affordable Wave Function Benchmark Method and Its Use to Test Density Functional Theory. *J. Chem. Theory Comput.* **2020**, *16*, 4416−4428.

(23) Drosou, M.; Mitsopoulou, C. A.; Pantazis, D. A. Spin-state energetics of manganese spin crossover complexes: Comparison of

single-reference and multi-reference ab initio approaches. *Polyhedron* **2021**, *208*, No. 115399.

(24) Drosou, M.; Mitsopoulou, C. A.; Pantazis, D. A. Reconciling Local Coupled Cluster with Multireference Approaches for Transition Metal Spin-State Energetics. *J. Chem. Theory Comput.* **2022**, *18*, 3538−3548.

(25) Kepp, K. P. Consistent descriptions of metal−ligand bonds and spin-crossover in inorganic chemistry. *Coord. Chem. Rev.* **2013**, *257*, 196−209.

(26) Kepp, K. P. *Transition Metals in Coordination Environments: Computational Chemistry and Catalysis Viewpoints*; Broclawik, E.; Borowski, T.; Radoń, M., Eds.; Springer International Publishing, 2019; pp 1−33.

(27) Atmani, C.; Hajj, F. E.; Benmansour, S.; Marchivie, M.; Triki, S.; Conan, F.; Patinec, V.; Handel, H.; Dupouy, G.; Gómez-García, C. J. Guidelines to design new spin crossover materials. *Coord. Chem. Rev.* **2010**, *254*, 1559−1569.

(28) Molnár, G.; Mikolasek, M.; Ridier, K.; Fahs, A.; Nicolazzi, W.; Bousseksou, A. Molecular Spin Crossover Materials: Review of the Lattice Dynamical Properties. *Ann. Phys.* **2019**, *531*, No. 1900076.

(29) Babilotte, K.; Boukheddaden, K. Theoretical investigations on the pressure effects in spin-crossover materials: Reentrant phase transitions and other behavior. *Phys. Rev. B* **2020**, *101*, No. 174113.

(30) Wang, M.; Li, Z.-Y.; Ishikawa, R.; Yamashita, M. Spin crossover and valence tautomerism conductors. *Coord. Chem. Rev.* **2021**, *435*, No. 213819.

(31) Janet, J. P.; Kulik, H. J. Predicting electronic structure properties of transition metal complexes with neural networks. *Chem. Sci.* **2017**, *8*, 5137−5152.

(32) Janet, J. P.; Chan, L.; Kulik, H. J. Accelerating chemical discovery with machine learning: simulated evolution of spin crossover complexes with an artificial neural network. *J. Phys. Chem. Lett.* **2018**, *9*, 1064−1071.

(33) Taylor, M. G.; Yang, T.; Lin, S.; Nandy, A.; Janet, J. P.; Duan, C.; Kulik, H. J. Seeing Is Believing: Experimental Spin States from Machine Learning Model Structure Predictions. *J. Phys. Chem. A* **2020**, *124*, 3286−3299.

(34) Nandy, A.; Duan, C.; Taylor, M. G.; Liu, F.; Steeves, A. H.; Kulik, H. J. Computational discovery of transition-metal complexes: from high-throughput screening to machine learning. *Chem. Rev.* **2021**, *121*, 9927−10000.

(35) Boča, R.; Linert, W. Is There a Need for New Models of the Spin Crossover? *Monatsh. Chem.* **2003**, *134*, 199−216.

(36) Koudriavtsev, A. B.; Linert, W. Spin crossover - an unusual chemical equilibrium. *J. Struct. Chem.* **2010**, *51*, 335−365.

(37) Vennelakanti, V.; Kilic, I. B.; Terrones, G.; Duan, C.; Kulik, H. Machine Learning Prediction of the Experimental Transition Temperature of Fe(II) Spin-Crossover Complexes. *J. Phys. Chem. A* **2024**, *128*, 204−216.

(38) Kench, T.; Rahardjo, A.; Terrones, G. G.; Bellamkonda, A.; Maher, T. E.; Storch, M.; Kulik, H. J.; Vilar, R. A semi-automated, high-throughput approach for the synthesis and identification of highly photo-cytotoxic iridium complexes. *Angew. Chem., Int. Ed.* **2024**, *63*, No. e202401808.

(39) Paulsen, H.; Trautwein, A. X. Spin Crossover in Transition Metal Compounds III. In *Topics in Current Chemistry*; Springer: Berlin, 2004; Vol. *235*, pp 197−219.

(40) Paulsen, H.; Schünemann, V.; Wolny, J. A. Progress in electronic structure calculations on spin-crossover complexes. *Eur. J. Inorg. Chem.* **2013**, *2013*, 628−641.

(41) Dittrich, B.; Ruf, E.; Meller, T. A feasibility study on obtaining d-orbital populations from aspherical-atom refinements on three spin crossover compounds. *Struct. Chem.* **2017**, *28*, 1333−1342.

(42) Cirera, J.; Via-Nadal, M.; Ruiz, E. Benchmarking Density Functional Methods for Calculation of State Energies of First Row Spin-Crossover Molecules. *Inorg. Chem.* **2018**, *57*, 14097−14105.

(43) Cirera, J.; Ruiz, E. Computational Modeling of Transition Temperatures in Spin-Crossover Systems. *Comments Inorg. Chem.* **2019**, *39*, 216−241.

(44) Römer, A.; Hasecke, L.; Blöchl, P.; Mata, R. A. A Review of Density Functional Models for the Description of Fe(II) Spin-Crossover Complexes. *Molecules* **2020**, *25*, 5176.

(45) Zheng, B.; Gu, G. X. Prediction of Graphene Oxide Functionalization Using Gradient Boosting: Implications for Material Chemical Composition Identification. *ACS Appl. Nano Mater.* **2021**, *4*, 3167−3174.

(46) Moses, I. A.; Joshi, R. P.; Ozdemir, B.; Kumar, N.; Eickholt, J.; Barone, V. Machine Learning Screening of Metal-Ion Battery Electrode Materials. *ACS Appl. Mater. & Interfaces* **2021**, *13*, 53355−53362.

(47) Duan, C.; Nandy, A.; Kulik, H. J. Machine Learning for the Discovery, Design, and Engineering of Materials. *Annu. Rev. Chem. Biomol. Eng.* **2022**, *13*, 405−429, DOI: 10.1146/annurev-chem-bioeng-092320-120230.

(48) Chan, C. H.; Sun, M.; Huang, B. Application of machine learning for advanced material prediction and design. *EcoMat* **2022**, *4*, No. e12194.

(49) Kipf, T. N.; Welling, M. Semi-Supervised Classification with Graph Convolutional Networks, 2017. https://doi.org/10.48550/arXiv.1609.02907.

(50) Bronstein, M. M.; Bruna, J.; LeCun, Y.; Szlam, A.; Vandergheynst, P. Geometric Deep Learning: Going beyond Euclidean data. *IEEE Signal Process. Mag.* **2017**, *34*, 18−42.

(51) Yang, C.; Lin, Y.; Liu, Z.; Sun, M. *Representation Learning for Natural Language Processing*; Liu, Z.; Lin, Y.; Sun, M., Eds.; Springer Nature: Singapore, 2023; pp 169−210.

(52) Khemani, B.; Patil, S.; Kotecha, K.; Tanwar, S. A review of graph neural networks: concepts, architectures, techniques, challenges, datasets, applications, and future directions. *J. Big Data* **2024**, *11*, 18.

(53) Maron, H.; Ben-Hamu, H.; Shamir, N.; Lipman, Y. Invariant and Equivariant Graph Networks, 2018. https://doi.org/10.48550/arXiv.1812.09902.

(54) Thomas, N.; Smidt, T.; Kearnes, S.; Yang, L.; Li, L.; Kohlhoff, K.; Riley, P. Tensor field networks: Rotation- and translation-equivariant neural networks for 3D point clouds, 2018. https://doi.org/10.48550/arXiv.1802.08219.

(55) Köhler, J.; Klein, L.; Noé, F. Equivariant Flows: sampling configurations for multi-body systems with symmetric energies, 2019. https://doi.org/10.48550/arXiv.1910.00753.

(56) Satorras, V. G.; Welling, E. H. M. In *E(n) Equivariant Graph Neural Networks*, Proceedings of the 38th International Conference on Machine Learning, 2021; pp 9323−9332.

(57) Satorras, V. G.; Welling, E. H. M. E(n) Equivariant Graph Neural Networks, 2021. https://github.com/vgsatorras/egnn (accessed December 09, 2023).

(58) Groom, C. R.; Bruno, I. J.; Lightfoot, M. P.; Ward, S. C. The Cambridge structural database. *Acta Crystallogr., Sect. B* **2016**, *72*, 171−179.

(59) Furness, J. W.; Kaplan, A. D.; Ning, A.; Perdew, J. P.; Sun, J. Accurate and numerically efficient r2SCAN meta-generalized gradient approximation. *J. Phys. Chem. Lett.* **2020**, *11*, 8208−8215.

(60) Mejía-Rodríguez, D.; Trickey, S. B. Spin-crossover from a Well-behaved, Low-cost meta-GGA Density Functional. *J. Phys. Chem. A* **2020**, *124*, 9889.

(61) Kresse, G.; Furthmüller, J. Efficient iterative schemes for ab initio total-energy calculations using a plane-wave basis set. *Phys. Rev. B* **1996**, *56*, 11169−11186.

(62) Bousseksou, A.; Molnár, G.; Salmon, L.; Nicolazzi, W. Molecular spin crossover phenomenon: Recent achievements and prospects. *Chem. Soc. Rev.* **2011**, *40*, 3313−3335.

(63) Gütlich, P.; Gaspar, A. B.; Garcia, Y. Spin state switching in iron coordination compounds. *Beilstein J. Org. Chem.* **2013**, *9*, 342−391.

(64) Cuéllar, M. P.; Lapresta-Fernández, A.; Herrera, J. M.; Salinas-Castillo, A.; Pegalajar, M. d. C.; Titos-Padilla, S.; Colacio, E.; Capitán-Vallvey, L. F. Thermochromic sensor design based on Fe(II) spin crossover/polymers hybrid materials and artificial neural networks as a tool in modelling. *Sens. Actuators, B* **2015**, *208*, 180−187.

(65) Nandy, A.; Duan, C.; Janet, J. P.; Gugler, S.; Kulik, Hj. Strategies and software for machine learning accelerated discovery in transition metal chemistry. *Ind. Eng. Chem. Res.* **2018**, *57*, 13973−13986.

(66) Zhao, W.; Li, Q.; Huang, X.-H.; Bie, L.-H.; Gao, J. Toward the prediction of multi-spin state charges of a Heme model by random forest regression. *Front. Chem.* **2020**, *8*, 162.

(67) Mejía-Rodríguez, D.; Albavera-Mata, A.; Fonseca, E.; Chen, D.-T.; Cheng, H.-P.; Hennig, R. G.; Trickey, S. B. Barriers to predictive high-throughput screening for spin-crossover. *Comput. Mater. Sci.* **2022**, *206*, No. 111161.

(68) Vennelakanti, V.; Taylor, M. G.; Nandy, A.; Duan, C.; Kulik, H. J. Assessing the performance of approximate density functional theory on 95 experimentally characterized Fe(II) spin crossover complexes. *J. Chem. Phys.* **2023**, *159*, No. 024120.

(69) McNaught, A. D.; Wilkinson, A. *IUPAC Compendium of Chemical Terminology*; International Union of Pure and Applied Chemistry, 2019.

(70) Prechelt, L. *Neural Networks: Tricks of the Trade*; Orr, G. B.; Mülle, K.-B., Eds.; Springer: Berlin, 1998; pp 55−69.

(71) Kingma, D. P.; Ba, J. Adam: A Method for Stochastic Optimization, 2017. https://doi.org/10.48550/arXiv.1412.6980.

(72) Krizhevsky, A.; Sutskever, I.; Hinton, G. E. ImageNet Classification with Deep Convolutional Neural Networks. *Commun. ACM* **2017**, *60*, 84−90.

(73) Pedregosa, F.; et al. Scikit-learn: Machine Learning in Python. *J. Mach. Learn. Res.* **2011**, *12*, 2825−2830.

(74) Huber, P. J. Robust Estimation of a Location Parameter. *Ann. Math. Stat.* **1964**, *35*, 73−101.

(75) Tsuchida, R. Absorption Spectra of Co-ordination Compounds. I. *Bull. Chem. Soc. Jpn.* **1938**, *13*, 388−400.

(76) Tsuchida, R. Absorption Spectra of Co-ordination Compounds. II. *Bull. Chem. Soc. Jpn.* **1938**, *13*, 436−450.

(77) Tsuchida, R.; Kobayasi, M. Absorption Spectra of Co-ordination Compounds. III. Special Bands of Chromium Complexes. *Bull. Chem. Soc. Jpn.* **1938**, *13*, 471−480.

(78) Kuroya, H.; Tsuchida; Absorption, R. Spectra of Co-ordination Compounds. IV. Ethylenediamine Cobaltic Complexes. *Bull. Chem. Soc. Jpn.* **1940**, *15*, 427−439.

(79) Yamada, S.; Tsuchida, R. Absorption Spectra of Coordination Compounds. V. The Hyperchromic Series of Ligands. *Bull. Chem. Soc. Jpn.* **1953**, *26*, 15−19.

(80) Nihei, M.; Shiga, T.; Maeda, Y.; Oshio, H. Spin crossover iron(III) complexes. *Coord. Chem. Rev.* **2007**, *251*, 2606−2621.

(81) Gaspar, A. B.; Seredyuk, M. Spin crossover in soft matter. *Coord. Chem. Rev.* **2014**, *268*, 41−58.

(82) Shatruk, M.; Phan, H.; Chrisostomo, B. A.; Suleimenova, A. Symmetry-breaking structural phase transitions in spin crossover complexes. *Coord. Chem. Rev.* **2015**, *289−290*, 62−73.

(83) Harding, D. J.; Harding, P.; Phonsri, W. Spin crossover in iron(III) complexes. *Coord. Chem. Rev.* **2016**, *313*, 38−61.

(84) Ferrando-Soria, J.; Vallejo, J.; Castellano, M.; Martínez-Lillo, J.; Pardo, E.; Cano, J.; Castro, I.; Lloret, F.; Ruiz-García, R.; Julve, M. Molecular magnetism, quo vadis? A historical perspective from a coordination chemist viewpoint. *Coord. Chem. Rev.* **2017**, *339*, 17−103.

(85) Hogue, R. W.; Singh, S.; Brooker, S. Spin crossover in discrete polynuclear iron(II) complexes. *Chem. Soc. Rev.* **2018**, *47*, 7303.

(86) Saito, Y.; Takemoto, J.; Hutchinson, B.; Nakamoto, K. Infrared studies of coordination compounds containing low-oxidation-state metals. I. Tris (2,2'-bipyridine) and tris (1,10-phenanthroline) complexes. *Inorg. Chem.* **1972**, *11*, 2003−2011.

(87) Sorai, M.; Seki, S. Phonon coupled cooperative low-spin $^1A^1$ high-spin $^5T^2$ transition in $[Fe(phen)_2 (NCS)_2]$ and $[Fe(phen)_2 (NCSe)_2]$ crystals. *J. Phys. Chem. Solids* **1974**, *35*, 555−570.

(88) Kulshreshtha, S. K.; Sasikala, R.; König, E. Calorimetric investigations of the low-spin $(^1A^1) \leftrightarrows$ high-spin $(^5T^2)$ transition in solid dithiocyanatobis(2,2'-BI-2-thiazoline iron(III). *Chem. Phys. Lett.* **1986**, *123*, 215−217.

(89) Paulsen, H.; Duelund, L.; Winkler, H.; Toftlund, H.; Trautwein, A. X. Free energy of spin-crossover complexes calculated with density functional methods. *Inorg. Chem.* **2001**, *40*, 2201−2203.

(90) Toftlund, H. Spin equilibrium in solutions. *Chem. Mon.* **2001**, *132*, 1269−1277.

(91) Sorai, M.; Nakano, M.; Miyazaki, Y. Calorimetric investigation of phase transitions occurring in molecule-based magnets. *Chem. Rev.* **2006**, *106*, 976−1031.

(92) Mortensen, S. R.; Kepp, K. P. Spin propensities of octahedral complexes from density functional theory. *J. Phys. Chem. A* **2015**, *119*, 4041−4050.

(93) Cook, L. J. K.; Kulmaczewski, R.; Mohammed, R.; Dudley, S.; Barrett, S. A.; Little, M. A.; Deeth, R. J.; Halcrow, M. A. A unified treatment of the relationship between ligand substituents and spin state in a family of iron (II) complexes. *Angew. Chem., Int. Ed.* **2016**, *55*, 4237−4331.

(94) Torgo, L.; Ribeiro, R. *Precision and Recall for Regression*; Discovery Science: Berlin, 2009; pp 332−346.

(95) Murray, K. S. *Spin-Crossover Materials: Properties and Applications*; Halcrow, M. A., Ed.; Wiley-Blackwell: Australia, 2013; pp 1−54.